Soft Matter

PAPER

View Article Online
View Journal | View Issue

Cite this: *Soft Matter*, 2021, **17**, 4304

Sequential and cellular detection of copper and lactic acid by disaggregation and reaggregation of the fluorescent panchromatic fibres of an acylthiourea based sensor†

Vivekshinh Kshtriya,[a] Bharti Koshti,[a] Deepak K. Pandey,[b] Sumit Kharbanda,[c] Chandra Kanth P,[d] Dheeraj K. Singh,*[b] Dhiraj Bhatia*[c] and Nidhi Gour‡*[a]

Received 10th January 2021,
Accepted 24th February 2021

DOI: 10.1039/d1sm00038a

rsc.li/soft-matter-journal

We report, for the first time, the self-assembly of an acyl-thiourea based sensor, *N*-{(6-methoxy-pyridine-2-yl) carbamothioyl}benzamide (**NG1**), with panchromatic fluorescent fibres and its dual-sensing properties for the sequential detection of Cu^{2+} ions and lactic acid. The panchromatic fibres formed by **NG1** were disrupted in the presence of Cu^{2+} ions and this was accompanied by a visible colour change in the solution from colourless to yellow. The addition of lactic acid to the **NG1** + Cu^{2+} solution, on the other hand, induced re-aggregation to fibrillar structures and the colour of the solution again changed to colourless. Hence, it may be surmised that the disaggregation and re-aggregation impart unique dual-sensing properties to **NG1** for the sequential detection of Cu^{2+} ions and lactic acid. The application of **NG1** as a selective sensor for Cu^{2+} ions and lactic acid has been assessed in detail by UV-visible and fluorescence spectroscopy. Furthermore, two structural variants of **NG1**, namely, **NG2** and **NG3,** were synthesized, which suggest the crucial role of pyridine in imparting panchromatic emission properties and of both pyridine and acyl-thiourea side chain in the binding of Cu^{2+} ions. The *O*-methoxy group plays an important part in making **NG1** the most sensitive probe of its structural analogs. Finally, the utility of **NG1** for the sequential and cellular detection of Cu^{2+} ions and lactic acid was studied in human RPE cells. The experimental results of the interaction of **NG1** with Cu^{2+} ions and lactic acid have also been validated theoretically by using quantum chemical calculations based on density functional theory (DFT). To the best of our knowledge, this is the first report wherein a dual sensor for Cu^{2+} ions and lactate ions is synthesized. More importantly, the aggregation properties of the sensor have been studied extensively and an interesting correlation of the photophysical properties of the probe with its self-assembling behavior has been elucidated.

Introduction

There is an ever-increasing need to develop new optical probes that could detect analytes with high sensitivity and good signal amplification. Various mechanisms are used to develop novel sensor molecules which include photo-induced electron transfer (PET),[1,2] intramolecular charge transfer (ICT),[3,4] fluorescence resonance energy transfer,[5] aggregation-induced emission (AIE),[6] aggregation-induced emission enhancement (AIEE),[7] metal to ligand charge transfer,[8,9] ligand to metal charge transfer,[10] and, donor–acceptor mechanisms,[11] and single electron transfer processes[12] and colourimetric detection.[13,14] Another very important sensing mechanism that can be utilized for the development of sensitive probes is disaggregation induced emission enhancement (DIEE).[15] The DIEE probes have very low fluorescence or are non-fluorescent in the aggregated state and the fluorescence is enhanced on disaggregation.[16] Disaggregation of the aggregated probe leads to a remarkable enhancement of emission and signal amplification. There are few literature reports that cite "disaggregation" as a mechanism for fluorescence enhancement;

[a] *Department of Chemistry, Indrashil University, Kadi, Mehsana, Gujarat, 382740, India. E-mail: nidhi.gour@indrashiluniversity.edu.in*
[b] *Department of Basic Sciences, Institute of Infrastructure Technology Research and Management, Ahmedabad, 380026, India*
[c] *Biological Engineering Discipline and Center for Biomedical Research, Indian Institute of Technology Gandhinagar, Palaj 382355, Gandhinagar, India*
[d] *Department of Science, School of Technology, Pandit Deendayal Petroleum University, Gandhinagar, Gujarat, India*

† Electronic supplementary information (ESI) available: Synthesis of **NG1**, **NG2** and **NG3** and its structural characterizations. It also contains accessory FTIR analysis, microscopic images and control studies. See DOI: 10.1039/d1sm00038a

‡ Past affiliation: Department of Medicinal Chemistry, Indian Institute of Advanced Research, Gandhinagar, Gujarat, 382426, India.

however, such reports are very limited, and not many research groups have explored this phenomenon.[17–20] Similarly the aggregation behaviour of the probe is seldom discussed, there are very few reports on the self-assembling properties[21,22] and microscopic analysis of the probe.[23,24] As a result of the poorly established concept, a proper interpretation of the data or an active application of the disaggregation for novel probe design has been hampered. Consequently, even if the ''disaggregation'' may be the real underlying mechanism, researchers remain unaware of it due to lack of microscopic analysis. Hence, the self-assembly/aggregation properties of the probe should be adequately discussed while deciphering the sensing mechanism. Herein, we report the self-assembly of a new acylthiourea based probe *N*-((6-methoxypyridin-2-yl)carbamothioyl)benzamide (**NG1**) with panchromatic fluorescent fibres extensively *via* the microscopic analysis. These self-assemblies are disrupted upon the addition of Cu^{2+}, and the disaggregation of the aggregated probe results in the golden yellow colour which could be visualized by the naked eye. This phenomenon is extensively studied by microscopic techniques like field emission-scanning electron microscopy (FE-SEM), atomic force microscopy (AFM), transmission electron microscopy (TEM) and fluorescence microscopy (Fig. 1).

The DIEE caused by the addition of Cu^{2+} ions to **NG1** has been used to design a sensor for the selective and sensitive detection of Cu^{2+}. Copper is an essential micronutrient; however, if the concentration of Cu^{2+} increases beyond a threshold, it causes deleterious effects on kidney, liver and gastrointestinal tracts and leads to diseases like Alzheimer's,[25] Parkinson's,[26,27] and Wilson's disease.[59] Chang *et al.* reported the fluorescent sensor for the selective detection of Cu^{2+} ions and citrate anion.[28] Hence, developing a selective and sensitive probe that could detect copper at a very minute level is of significant importance. It was further noted that the addition of lactic acid causes fluorescence quenching of the **NG1**–Cu^{2+} complex; hence, the novel probe can also be used for the sequential detection of Cu^{2+} and lactate. Lactic acid is also very harmful at concentrations above a threshold and many diseases like mitochondrial diseases, cerebral ischemia and cancer are associated with high lactate levels in the blood.[29] Combined experimental tools (UV-visible spectroscopy, fluorescence spectroscopy, Fourier Transform Infrared (FTIR) Spectroscopy, and Nuclear Magnetic Resonance (NMR) spectroscopy and quantum chemical calculations based on density functional theory (DFT)) were used for deciphering the sequential identification of copper II (Cu^{2+}) and lactic acid by fluorescent probe **NG1**.

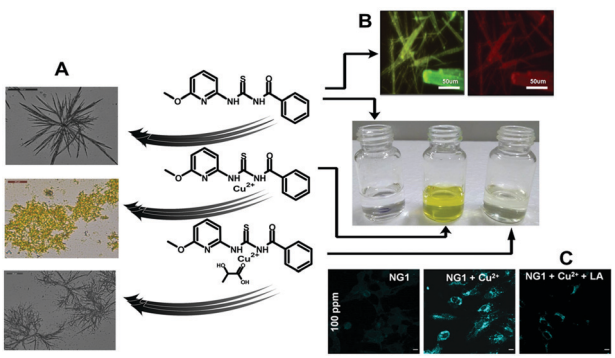

Fig. 1 A diagrammatic representation of the aggregation properties of **NG1** and its implications in the sequential detection of Cu^{2+} and Lactate. (A) Optical microscopy images of **NG1**: Aggregated state (top) **NG1** alone; disaggregated state (middle) **NG1** + $Cu^{2+}$and re-aggregated state (bottom) **NG1** + Cu^{2+} + Lactic acid (LA); scale bar: 20 μm. Colourimetric change in the vial containing **NG1** upon the addition of Cu^{2+} and Cu^{2+} + LA; (B) self-assembly of **NG1** with panchromatic fibres; (C) sequential cellular detection of Cu^{2+} in retinal pigment epithelial (RPE) cells using **NG1**, Scale bar: 10 μm.

Results and discussion

The structural basis for the design of the **NG1** molecule was the acyl thiourea side chain. There are literature reports that reveal the exceptional photophysical properties of acyl thiourea based conjugates and hence they can be efficiently used as a sensor.[30–35] Our group has been actively studying the self-assembled structures formed by single amino acids,[36] peptides[37–41] and heterocycles.[42] Our recent research on pyridothiazole based conjugate revealed its self-assembly to structures and a subsequent change in the photophysical properties due to aggregation. The aggregation-induced emission enhancement (AIEE) properties of this conjugate imparted it an exceptional ability to selectively sense amyloid.[42] Hence, we were motivated to design a novel acyl thiourea conjugate **NG1** and assess its aggregation properties to decipher the underlying mechanism of sensing from an aggregation perspective. The structure of **NG1** was designed with the aim to make it a more appropriate sensor. The sulphur and oxygen atoms present in the acyl thiourea side chain of **NG1** were conjugated to *O*-methoxy pyridine. This conjugation imparted more electron-donating capacity to the oxygen and sulphur atoms, through which they can tightly bind with the divalent metal ions. Due to the presence of an aromatic ring in the structure, it was also expected that **NG1** would tend to aggregate and self-assemble to fibre like structures *via* pi–pi stacking as reported previously.[43]

The chemical synthesis of **NG1** was carried out in one step by condensation reaction between benzoyl isothiocyanate and 2-Amino-6-methoxypyridine as shown in Scheme 1. The chemical structure of **NG1** was characterized by ^{1}H (Fig. S15, ESI†) and ^{13}C-NMR (Fig. S16 and S17, ESI†), and LCMS,

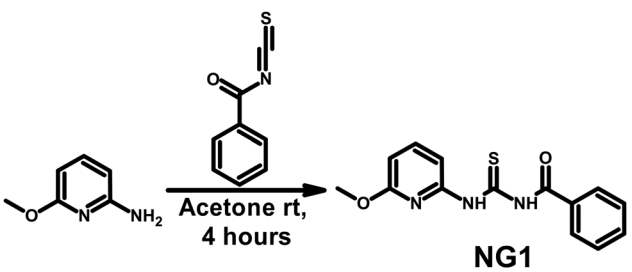

Scheme 1 Schematic representation of the synthesis of the probe **NG1**.

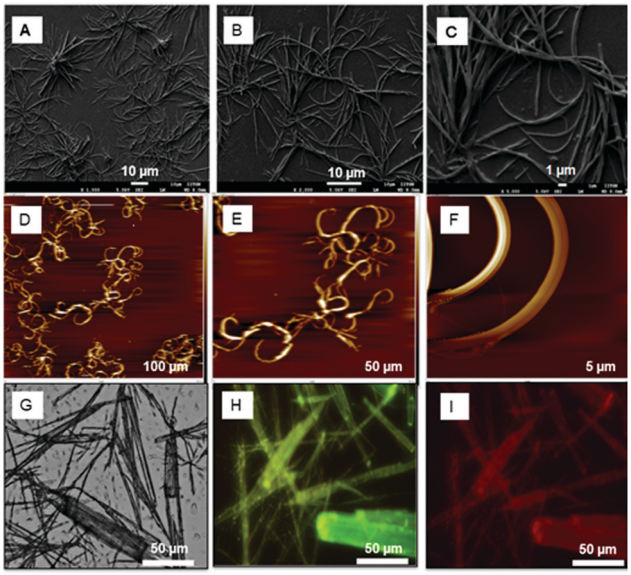

Fig. 2 Microscopy images of self-assembled structures of **NG1** (1 mM) in 70% aqueous methanol. (A) SEM at 10 μm scale; (B) SEM at 5 μm scale; (C) SEM at 1 μm scale; (D) AFM at 100 μm scale; (E) AFM at 50 μm scale bar; and (F) AFM at 5 μm scale; (G) bright field images of the fibres of **NG1,** (H) under the green filter, and (I) under the red filter.

(Fig. S18, ESI†) and its purity was ascertained through HPLC (Fig. S19, ESI†).

Once the chemical structure of **NG1** was characterized thoroughly, we studied the self-assembling properties of **NG1**. For self-assembly studies, **NG1** was dissolved at 1 mM concentration in 70% aqueous methanol. The scanning electron microscopy (SEM) image of **NG1** reveals its assembly to fibre like morphologies. The diameter of these fibres was 200–400 nm and the length varied to several micron ranges (Fig. 2A and C). The AFM micrograph studies further confirmed the fibrillar structures formed by **NG1** (Fig. 2D–F).

The fibres formed by the self-assembly of **NG1** were also studied extensively *via* optical and fluorescence microscopy. It was noted that **NG1** fibres exhibit fluorescence. The fibres revealed green emission under the FITC filter (Ex 480/40 Em 527/30) and red emission under the rhodamine filter (Ex 546/10 Em 585/40). The emission spectra of **NG1** also changed in accordance with the excitation wavelength through fluorescence spectroscopy (Fig. S14, ESI†). From the emission spectra, it can be interpreted that **NG1** shows maximum fluorescence under blue excitation followed by green and the lowest was red. The fluorescence microscopy (Fig. 2G–I, ESI†) and fluorescence spectroscopy (Fig. S13, ESI†) clearly suggest that **NG1** assembled to panchromatic aggregates which show tunable emission albeit with low fluorescence intensities. Furthermore, we also synthesized structural analogs of **NG1,** namely **NG2** and **NG3,** which does not have the *O*-methoxy group and the pyridine group, respectively, to decipher the structural basis for the formation of panchromatic self-assemblies. It was noted that **NG2** also assembles to panchromatic fibres (Fig. 2G–I); however, since **NG3** does not have a pyridine group, it does not possess panchromatic properties (Fig. S4, ESI†). Hence, the pyridine group plays a crucial role in the panchromatic emission.

There are reports in literature wherein acyl thiourea derivatives have been used as a probe for the detection of Cu^{2+} ions.[33–35] Hence, we were motivated to assess the effect of Cu^{2+} ions on the aggregation properties of **NG1.** Interestingly, when Cu^{2+} ions were added to these fibres, disruption of the fibril assembly could be observed. It was also evident that the colourless solution of **NG1** changed to golden yellow on the addition of Cu^{2+}. When EDTA, a well know metal chelator, was added to the **NG1** + Cu^{2+} complex, the yellow colour changed to colourless and the fiber structures were regenerated (Fig. S20, ESI†). This experiment suggested the crucial role of disaggregation in attributing unique photophysical properties to **NG1.** The disaggregation induced colour production (DICP) was very intriguing to us and we decided to first assess whether this colour change can be produced only by Cu^{2+} or if it can be observed with other metal ions as well. To assess the specific sensing properties of **NG1** for Cu^{2+}, experiments were performed by co-incubating **NG1** with a series of metal ions commonly found in water. Metal-ion binding studies of **NG1** were carried out following the method described in the experimental section using the metal ions, such as Cu^{+}, Na^{+}, K^{+}, Ba^{2+}, Ca^{2+}, Mg^{2+}, Cr^{3+}, Mn^{2+}, Co^{2+}, Ni^{2+}, Zn^{2+}, Pb^{2+}, Sr^{2+}, Fe^{2+}, Fe^{3+}, and Cu^{2+} ions. As can be surmised from Fig. S6 in the ESI,† **NG1** selectively detected only Cu^{2+} ions and the colour of the solution in a vial containing **NG1** + Cu^{2+} changed from colourless to yellow (Fig. S6, ESI†). Furthermore, the microscopic images also revealed that the panchromatic fibres formed by **NG1** could only be disrupted by Cu^{2+} and not by any other ions (Fig. S3, ESI†) suggesting the crucial role of disaggregation in this specific sensing. In addition, an interference assay was also performed by mixing all the metal ions except Cu^{2+} with **NG1.** Notably, there was no visible change in the colour of the solution even in the presence of all metal ions. However, when Cu^{2+} ions were added to this mixture, the colourless solution changed to yellow. As revealed by the colorimetric response, **NG1** produced yellow colour only in the presence of Cu^{2+} and was least affected by the presence of other types of common ions (250 ppm: Na^{+}, Cu^{+}, Fe^{3+}, Mn^{2+}, K^{+}, Mg^{2+}, Ca^{2+}, and Cr^{3+} ions). Hence, it can be inferred that **NG1** shows optimal activity with negligible interference by other ions (Fig. S6, ESI†). The microscopic study of fibres formed by **NG1** also reveals that only Cu^{2+} could cause disruption of fibres and they remain unaffected by the addition of a mixture of other ions (data not shown) confirming a definite correlation of **NG1** aggregation properties with its photophysical characteristics.

The results of the interaction of **NG1** with Cu^{2+} were further validated using UV–visible spectroscopy studies. The UV visible spectra of 50 ppm solution of **NG1** reveal a broad peak with maxima from 290 to 320 nm. When 50 ppm Cu^{2+} was added to this solution, the peak shifted from 310 nm to 339.5 nm. There was also a slight enhancement of broad peak in the range of 400–450 nm which corresponded well with the yellow colour produced in the solution due to interaction between **NG1** and Cu^{2+} ions and may be attributed to intramolecular charge transfer (ICT) transition (Fig. 3A). To study the interaction of **NG1** with Cu^{2+} ions in more detail, the absorption spectra of

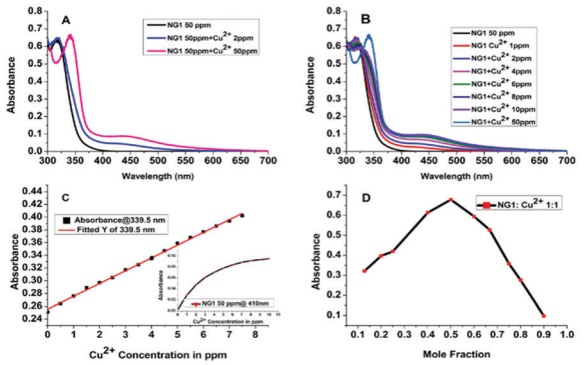

Fig. 3 (A) UV-visible spectra of probe **NG1** with and without Cu^{2+} at 50 ppm concentration; (B) UV-visible spectra of probe **NG1** after the sequential addition of Cu^{2+}; (C) LOD of probe **NG1** for detecting the presence of Cu^{2+} at 339.5 nm, (inset) plot of absorbance *vs.* Cu^{2+} at 410 nm; (D) Job's plot drawn taking a fixed concentration of probe **NG1** and varying concentrations of Cu^{2+} ions revealed 1 : 1 stoichiometry between **NG1** and Cu^{2+}.

the probe were studied in the presence of different ppm levels of Cu^{2+} ions by UV-visible spectroscopy. As shown in Fig. 3A, **NG1** exhibited a maximum absorption at ~310–320 nm. On the gradual addition of Cu^{2+} ions, the absorption intensity shifts from 320 nm to nearly 340–370 nm. There was more and more red shift as the concentration of Cu^{2+} ions (0–50 ppm) was gradually increased and this was attributed to the formation of the **NG1**–Cu^{2+} complex (Fig. 3B). The interaction is replicated by the visual colour change from colourless to yellow.

To investigate the sensitivity of the synthesized probe **NG1** towards Cu^{2+} ions, a straight-line plot was drawn between the concentration of Cu^{2+} and absorbance at 339.5 nm (Fig. 3C). The plot shows the linear relationship in the concentration range between 2.5 and 10 ppm. The limit of detection (LOD) was calculated using the following formula.

$$\mathrm{LOD} = \frac{3\sigma}{\text{Slope of calibration curve}}$$

where σ is the standard deviation.

LOD was found to be 1.5 ppm from the plot of absorbance *vs.* Cu^{2+} ion concentration for absorbanceat 339.5 nm while it was calculated to be 8.7 ppm (3.5 μM) for the absorbanceat 410 nm which corresponded to yellow colour (Fig. S6, ESI†). In conclusion, the convenient detection limit for the newly synthesized probe **NG1** is 1.5 ppm (0.6 μM) for Cu^{2+} ions, which is much lower according to the maximal permitted level of Cu^{2+} ions (15 μM) in water considering the highest safety standards. The short response time and high selectivity of the probe **NG1** in visual inspection could be accounted for its strong and specific affinity towards Cu^{2+} ions. (Fig. 3C, inset).

Furthermore, Job's plots were constructed to demonstrate the complexation between Cu^{2+} and probe which indicated a stoichiometry of 1 : 1 complexation between Cu^{2+} ions and **NG1**. The 1 : 1 binding stoichiometry suggests bis-coordination of Cu^{2+} ions *via* nitrogen and sulphur atoms present on the probe **NG1** (Fig. 3D). Moreover, the interaction and binding behaviour between **NG1** and Cu^{2+} ions were also evinced *via* FTIR presented in the ESI† (Fig. S8). The FTIR spectrum supported the change in characteristic peaks of probe **NG1** in the aromatic region (1450–1650 cm^{-1}) due to interaction *via* nitrogen and sulfur atoms present on **NG1** with Cu^{2+} ions and proved the formation of the **NG1**–Cu^{2+} complex. Thus, the present study realizes that the probe **NG1** can be used for the simultaneous detection of Cu^{2+} ions in real water samples as well as it could potentially be used for sensing Cu^{2+} ions in mammalian cells and organisms.

To assess the role of deprotonation in the **NG1**–Cu^{2+} complex formation, we also studied the role of pH in this complexation. Originally, the pH of the **NG1** solution was 7.2. After the addition of Cu^{2+}, the pH remains unchanged. To assess the effect of pH on the sensing of Cu^{2+} ions, **NG1** pH was made acidic at pH 5.0 and also basic at pH 9.0. Also, **NG1** was dissolved in PBS buffer at pH 7.4 and subsequently, Cu^{2+} was added under acidic, basic and physiological conditions. In all these vials, **NG1** was able to sense Cu^{2+} and produced yellow colour, indicating that pH does not affect sensing properties and ruled out the role of deprotonation in sensing (Fig. S10, ESI†). It further demonstrates the efficacy of **NG1** to be a very good sensor for the detection of Cu^{2+} even under acidic and basic conditions and its utility in real sample analysis of industrial water.

Once the sensitivity and selectivity of the probe **NG1** were ascertained by colorimetry, the fluorescence assay was performed in the presence of Cu^{2+} ions since self-assembly of **NG1** revealed the formation of fibres showing panchromatic emission. When **NG1** was excited at 353 nm, the emission spectra were obtained with the maxima at 450 nm. When Cu^{2+} ions were added in increasing concentration there was a significant enhancement in the fluorescence intensity and the graph exhibited a red-shift towards 470 nm (Fig. 4A). Interestingly, from UV studies, it can be assessed that the peak shift of **NG1** occurs from 310 to 370 nm on the addition of Cu^{2+} ions. Hence, excitation at 353 nm might be attributed to this absorbance.

In our body, copper mainly exists in the form of copper citrate. However, copper also plays an important role in regulating blood lactate levels and forms copper lactate complex inside the body.[35] Hence, we decided to perform titration studies on the interaction

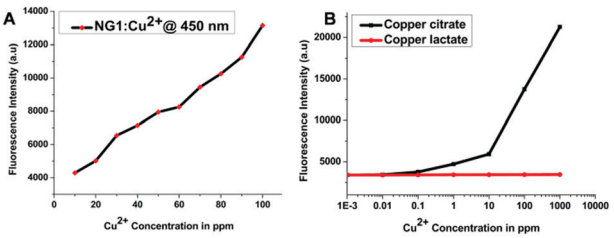

Fig. 4 (A) The curve plotted with the fluorescence intensity of **NG1** (250 ppm) at 450 nm *versus* Cu^{2+} ion concentration (0.0001 ppm–100 ppm) showed a steady increase in fluorescence as the concentration of Cu^{2+} ions was increased; and (B) fluorescence graph shows no enhancement on the addition of copper lactate to **NG1** in increasing amount, on the other hand, copper citrate showed a steady increase in fluorescence with increase in its concentration.

of **NG1** with copper citrate and copper lactate. Interestingly, while Cu(II) citrate showed a steady increase in fluorescence, the Cu(II) lactate salt was not able to bind **NG1** and no increase in fluorescence was observed. This study indicated that the Cu(II) lactate complex was more stable and hence Cu^{2+} ions could not form a complex with **NG1** and induce a colour change (Fig. 4B).

Hence, motivated by these results, we decided to assess the application of **NG1** for the sequential detection of both Cu^{2+} ions and lactate ions. The UV visible experiment of the **NG1**–Cu^{2+} complex with lactic acid at high concentrations revealed that the yellow colour of the **NG1** + Cu^{2+} complex fades to a nearly colourless solution (Fig. 5A and Fig. S11, ESI†). Interestingly, the yellow colour of the **NG1**–Cu^{2+} complex remains unaffected by excess addition of other counter anions like oxalate and citrate and only lactate was able to decolourize the yellow solution (data not shown). Furthermore, UV-Visible titration of the **NG1**–Cu^{2+} complex with lactic acid was carried out which revealed a decrease in absorbance on the addition of increasing concentration of lactic acid to the 50 ppm **NG1**:Cu^{2+} yellow complex from 0 to 500 ppm (Fig. 5B). Notably, the absorbance at both 339.5 nm and 410 nm decreased as can be deciphered from plots shown in Fig. 5B and C, respectively.

Furthermore, to assess the role of self-assembly of **NG1** in the sequential detection of Cu^{2+} and lactate, optical microscopy studies of fibres formed by **NG1** were performed in the presence of Cu^{2+} and lactic acid. It was noted that the fibres which were disrupted by the addition of Cu^{2+} were regenerated on the sequential addition of lactic acid. This experiment clearly revealed a crucial role of disaggregation in inducing yellow colour on the addition of Cu^{2+} and re-aggregation in changing it back to colourless on the addition of lactic acid.

Transmission Electron Microscopy was also performed to observe the morphologies of the structures formed by **NG1** + Cu^{2+} at a higher magnification. At a higher magnification too, **NG1** reveals clustered fibres (Fig. 6A). When **NG1** + Cu^{2+} sample was observed, a disruption in the fiber aggregates could be seen (Fig. 6B). The organic layer appears to be dissolved by Cu^{2+} and hence SAED was done to decipher if this organic layer has some crystalline characteristics (Fig. 6C). However, no crystalline morphologies, as well as reduced Cu(0) nanoparticles, could be observed.

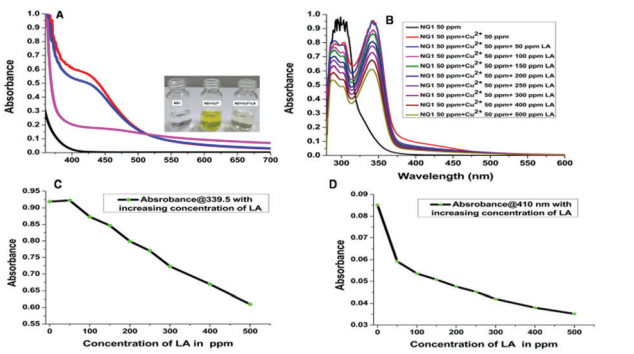

Fig. 5 (A) UV-visible spectra recorded from 370 to 700 nm at high concentration of **NG1** (250 ppm) (black); with Cu^{2+} (1 : 1) (red); after the addition of lactic acid (LA) (1 : 1;10) (pink) showing the change of yellow colour to colourless; (B) the UV spectra of **NG1** (50 ppm), **NG1**–Cu^{2+} complex (50 ppm : 50 ppm) and varying concentrations of LA to assess visual colour change; (B) UV-visible spectra of **NG1** (50 ppm) in the presence of Cu^{2+} ions (50 ppm) and varying concentrations of lactic acid (0 ppm–500 ppm); (C) the UV spectra of the **NG1**–Cu^{2+}complex against varying concentrations of lactic acid from 0 to 500 ppm at wavelength 339.5 nm and (D) the UV spectra of **NG1**–Cu^{2+} complex against a varying concentrations of lactic acid from 0 to 500 ppm at wavelength 410 nm for detecting decrease in yellow colour.

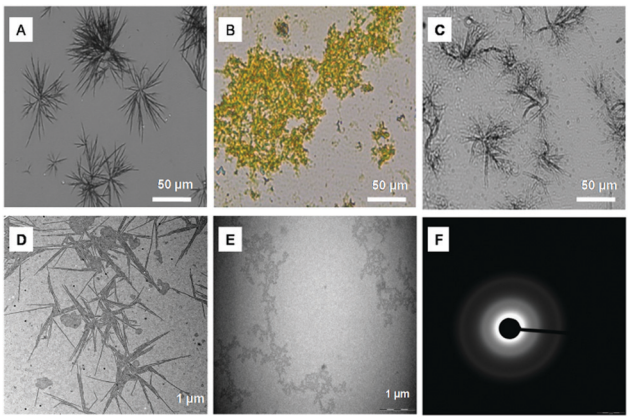

Fig. 6 Microscopy image of **NG1** (1 mM) in 70% aqueous methanol. (A) **NG1** alone; (B) **NG1** + Cu^{2+}(1 : 1); (C) **NG1** + Cu^{2+}+ lactic acid (1 : 1 : 5); (D) TEM image of **NG1**; (E) TEM image of **NG1** + Cu^{2+}(1 : 1); and (F) SAED pattern of **NG1** + Cu^{2+} showing the non crystalline nature.

To know more about the molecular packing present in **NG1** non-assembled, self-assembled, and **NG1** + Cu^{2+} complex we studied its XRD in powder mode (Fig. S12, ESI†). The study revealed that non-assembled **NG1** is more crystalline in nature when compared to the self-assembled material. There were more peaks observed in the case of non-assembled material due to its more uniform lattice arrangement while in the case of self-assembled **NG1**, molecules are arranged through weak interaction force such as hydrogen bonding, and van der Waals and pi–pi interactions due to which the properties of the material will change towards more amorphous rather than crystalline nature.[45] The different XRD patterns of the non-assembled and self-assembled **NG1** also indicate their different morphologies. When Cu^{2+} is added, the molecular packing present in **NG1** is further disturbed, resulting in obvious changes in the 2θ value. The disappearance of peaks arising from **NG1** on the addition of Cu^{2+} indicates complex formation and a completely different molecular packing and morphology.[44] These results also further supported the SAED results obtained using TEM for the **NG1** + Cu^{2+} complex.

Furthermore, to understand the role of acyl thiourea side chain present in **NG1**, the photophysical properties of two other structural analogs of this probe, namely, **NG2** and **NG3** were studied in the presence of Cu^{2+}. Interestingly, both probes **NG1** and **NG2** show selective sensing for Cu^{2+} ions. However, probe **NG3** showed very little sensitivity for Cu^{2+} ions. It also did not exhibit panchromatic behavior. Hence, the crucial role of pyridine in sensing as well as in panchromatic emission may be deciphered. The order of sensitivity of **NG1** for the detection

of Cu^{2+} ions was **NG1** > **NG2** > **NG3**. Furthermore, since **NG3** could also sense Cu^{2+} ions, albeit with low sensitivity, it may be inferred that the acyl thiourea moiety can also participate in complex formation. Since **NG1** revealed higher sensitivity as compared to **NG2**, a crucial role of the –*O*-methoxy group for increasing sensitivity could also be surmised. The methoxy group is known to have electron releasing properties. The lone pairs of the methoxy groups present in **NG1** may be involved in resonance and could attribute to an increase in the electron density around the sulphur and oxygen atoms. Hence, sulphur and oxygen atoms in **NG1** can easily donate their lone pairs of electrons to Cu^{2+} and cause its effective binding leading to the yellow colour complex formation.

Cellular detection of Cu^{2+} and lactate using the NG1–Cu^{2+} complex

The *in vitro* sensing capabilities for **NG1**–Cu^{2+} were further explored by testing its capacity to sense Cu^{2+} and lactate in mammalian cells.[46,47] The application of the **NG1**–Cu^{2+} complex was tested in living cells by using MTT cytotoxicity assay and cellular imaging. Cell viability was measured by measuring the absorbance of MTT at 570 nm and calculating the ratio of absorbance of cells treated with respective compounds to that of control untreated cells. The results as shown in Fig. 7A indicate that **NG1** compounds have minimum cytotoxicity in cells (~80% cell viability), strongly suggesting that these compounds can be further exploited for cellular imaging applications. MTT assays were carried out using a stock solution of 500 : 500 ppm **NG1**:Cu^{2+}. The stock was serially diluted and cells were grown in wells containing 25, 50, 75, 100, 150, 200, and 250 ppm of the **NG1** : Cu^{2+} complex. To test for cell permeability and fluorescence properties of **NG1** molecule in cells, experiments were carried out using the retinal pigmented epithelial (RPE1) cells. The cells were pulsed with **NG1** in the absence or presence of different concentrations of Cu^{2+} for 15 mins, fixed and imaged using a confocal microscope. Following *in vitro* data, imaging of fixed cells using a confocal microscope displayed that these compounds are permeable in cells and show bright blue fluorescence in the blue filter (shown in Fig. 7B). From the fluorescence spectroscopy analysis, it was evident that the fluorescence of **NG1** enhances with increase in the concentration of Cu^{2+} added to it. Hence, it was expected that when the cells are visualized under a blue filter (Em 450–470 nm) the fluorescence of the dye **NG1** would be highly enhanced in the presence of exogenous Cu^{2+} (Fig. 7A). Indeed, similar observations could be noted *via* cell imaging analysis and there was a remarkable enhancement of fluorescence on the addition of Cu^{2+}. This enhancement in the cellular intensity of dye was rescued to background levels in the presence of lactic acid, indicating the potential of the dye to sense both Cu^{2+} and lactate from cells (Fig. 7C).

Theoretical studies by DFT calculations

Furthermore, to perceive a greater insight into the complex formation by **NG1** and its structural analogs **NG2** and **NG3** with Cu^{2+} and lactic acid, we resorted to validate theoretically the experimental results using quantum chemical calculations

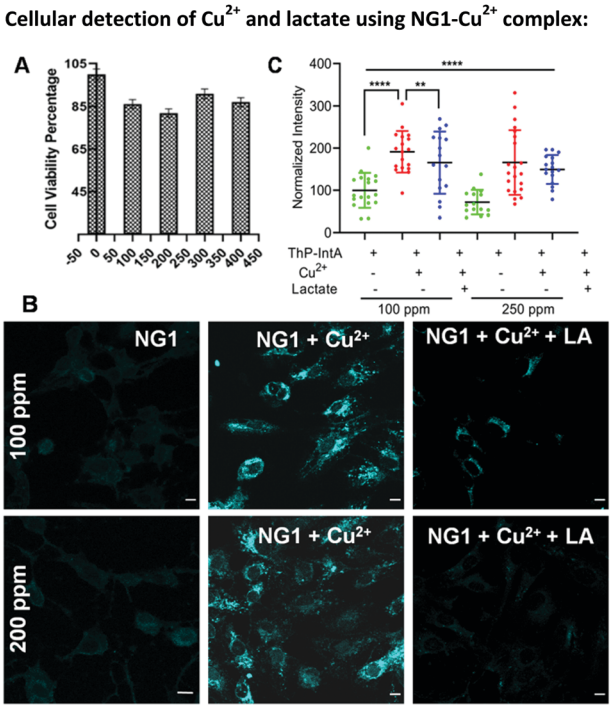

Fig. 7 Cytotoxicity measurements and cellular imaging of Cu^{2+} and lactic acid in human cells. (A) The MTT assay of RPE1 cell using **NG1** molecule. Cells were treated with different concentrations of **NG1** and the cell viability was calculated using the MTT assay (n = 2 experiments with 10 000 cells under each condition); (B) retinal epithelial pigmental cells (RPE1) were pulsed with 100 and 250 ppm of **NG1** dye in the absence or presence of Cu^{2+} in a 1 : 1 ratio of dye : Cu^{2+}. Furthermore, the cells were incubated with lactate in presence of dye and Cu^{2+} for 15 min at 37 °C, fixed with paraformaldehyde, and imaged using a confocal microscope with a 405 nm excitation laser and images were acquired using broad width band-pass filters. (C) The images were further quantified using image-J for the cellular intensity of dye under various conditions and the normalized intensity plotted in the right figure. Scale bar: 10 μm.

based on density functional theory (DFT). In various fields of science, DFT-based quantum chemical calculations are used to elucidate the electronic structures of numerous chemical species and have become an excellent tool for solving interesting chemical problems and reaction mechanisms.[48–51,58] Here, in the present study, we first conducted a comparison study on three probes (**NG1**, **NG2**, and **NG3**) and their complex formation with Cu^{2+} ions and lactic acid. DFT calculations were performed at the B3LYP/6-311++G(d,p) level of theory for these probes and their complexes in the gaseous phase. The vibrational frequencies were also calculated for all the studied structures, where the optimization converged successfully to the shallow local minima on the potential energy surface, which was confirmed by the absence of negative/imaginary vibrational frequencies. Fig. 8 shows the ground state optimized geometries of all the three probes and their association with Cu^{2+} as well as lactic acid. The binding energy (BE) of these complexes are elucidated as:

$$BE = E_{complex} - \sum E_{individual} \quad (1)$$

where $E_{complex}$ represents the ground state energy of the complex and $E_{individual}$ indicates the sum of the ground state energies of all the molecules in a particular complex. The BE of

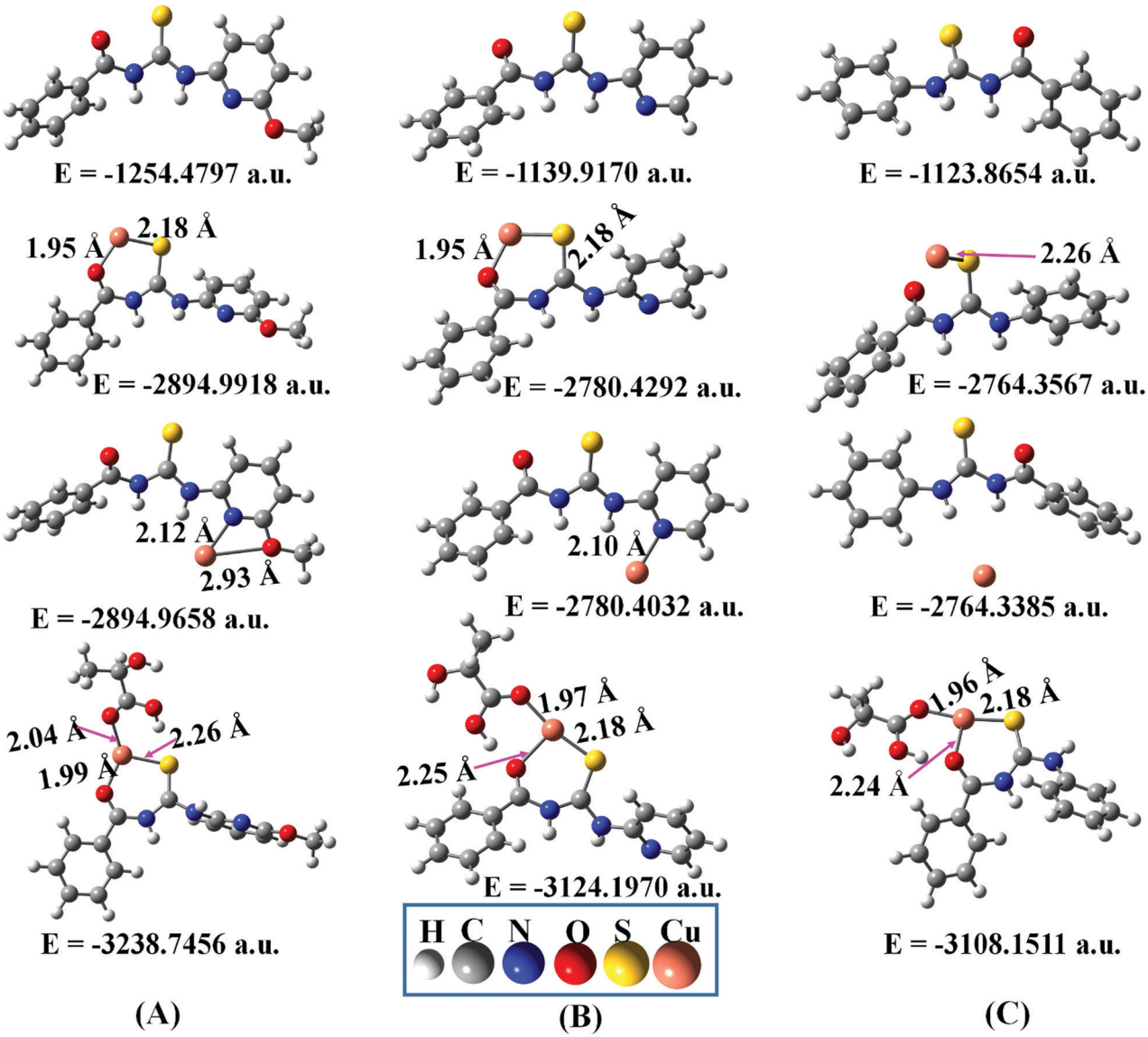

Fig. 8 DFT computed optimized geometries of (A) **NG1**, configuration 1, configuration 2 and configuration 1 + lactic acid, (B) **NG2**, configuration 1, configuration 2 and configuration 1 + lactic acid, and (C) **NG3**, configuration 1, configuration 2 and configuration 1 + lactic acid with their optimized energy in Hartree.

all the optimized structures is presented in curly braces in Table 1.

Initially, the pristine probes, *i.e.*, **NG1**, **NG2**, and **NG3** were optimized using DFT calculations. Based on energetic stability, **NG1** was found to be the most stable ligand. To make a better comparison, along with **NG1**, the other two probes (**NG2** and **NG3**) were also interacted with Cu^{2+} and lactic acid (Fig. 8). Two possible configurations were identified for the study of the interaction of Cu^{2+} with these probes. Here, configuration 1 indicates when Cu^{2+} interacts with the sulphur atom of these probes and configuration 2 denotes when Cu^{2+} interacts near the nitrogen atoms of the probe as can be seen in Fig. 8. After the interaction and geometry relaxation process, it is noteworthy that among all the six complexes (with Cu^{2+}),

Table 1 Optimized energy (in Hartree) and binding energy (in kcal mol^{-1}) of the complexes **NG1**, **NG2**, and **NG3**. The binding energies in kcal mol^{-1} are provided in curly braces

Ligands	Optimized energy	Configuration 1 (Cu^{2+} is interacting near sulphur atom)	Configuration 2 (Cu^{2+} is interacting near nitrogen atom)	Configuration 1 With lactic acid
NG1	−1254.4797	−2894.9918 {−25.07}	−2894.9658 {−8.71}	−3238.7456 {−87.05}
NG2	−1139.9170	−2780.4292 {−25.06}	−2780.4032 {−8.73}	−3124.1970 {−120.91}
NG3	−1123.8654	−2764.3567 {−11.97}	−2764.3385 {−0.55}	−3108.1511 {−124.46}

Cu^{2+} tends to strongly bind with the sulphur atom of all the studied probes (**NG1**, **NG2** and **NG3**) *i.e.*, in configuration 1 as shown in the second row in Fig. 8. This trend is also confirmed from the binding energies which are higher for configuration 1 than configuration 2 in all the studied probes. The BE calculations for all the complexes (with Cu^{2+}) indicate that configuration 1 of probe **NG1** is the most stable complex. Nevertheless, the BE of configuration 1 of **NG1** is -25.07 kcal mol^{-1} which is slightly higher in comparison to configuration 1 of the **NG2** complex. This small energy difference is considerable here because in experimental observation all the three probes give yellow colour after incorporating the Cu^{2+} but the only key difference between these three probes was their sensitivities. For probe **NG1**, the presence of only 1.5 ppm concentration of Cu^{2+} causes the occurrence of yellow colour but in the case of other probes (**NG2** and **NG3**), yellow colour appears only after the incorporation of high Cu^{2+} concentration. So, for further studies, we have selected configuration 1 of **NG1** on the basis of BE to validate our experimental findings.

Here, Cu^{2+} strongly interacts with the oxygen and sulfur atoms having a bond length of 1.95 Å and 2.18 Å, respectively (see second geometry of Fig. 8A). In configuration 2 (all three probes), Cu^{2+} is weakly coordinated with nitrogen and oxygen atoms as their bond length increased on the interaction (see Fig. 8). We have also optimized the dimer like structure of **NG1** with a single Cu^{2+} atom to check the assembly of Cu^{2+} with more **NG1** molecules and almost similar structural features are found as in the single case where Cu^{2+} interacts with the S atom of another **NG1** (Fig. 9C).

As experimentally observed, the interaction of Cu^{2+} with **NG1** yields a yellow-coloured complex but when lactic acid is incorporated within this complex, the yellow colour is suppressed. To understand this behavior, we have introduced a molecule of lactic acid with this stable configuration 1 of **NG1** and the optimized geometry can be seen at the bottom of Fig. 8A (vertically). From Fig. 8A (comparing the structure of second and fourth geometry from the vertical position), it is noticeable that Cu^{2+} is strongly binding with the sulfur and oxygen atoms of **NG1** through 2.18 Å and 1.95 Å, respectively. However, upon complex formation with lactic acid, both the bond strengths get weakened and the bond lengths are calculated to be 2.26 Å and 1.99 Å, respectively. Also, it can be noticed from Fig. 9A that Cu^{2+} forms a strong bond (2.20 Å) with the oxygen atom of –C═O of the carboxylic group in a lactic acid molecule. But after the complex formation of configuration 1 with lactic acid, this bond gets stronger with a new bond length of 2.04 Å as can be seen in Fig. 9B. Another noticeable feature is the least BE of this complex of **NG1** (configuration 1 + lactic acid) in comparison to the other complexes. The BE of this complex is -87.05 kcal mol^{-1} which is much lower than the -95.86 kcal mol^{-1} and -112.49 kcal mol^{-1} for configuration 1 + lactic acid of probes **NG2** and **NG3**, respectively. Hence, this BE and changes in bond lengths give a clear indication of Cu^{2+} binding with lactic acid and hence altering the properties of the **NG1** + Cu^{2+} complex due to the formation of copper lactate and resulting decolourization. Furthermore, electrostatic potential

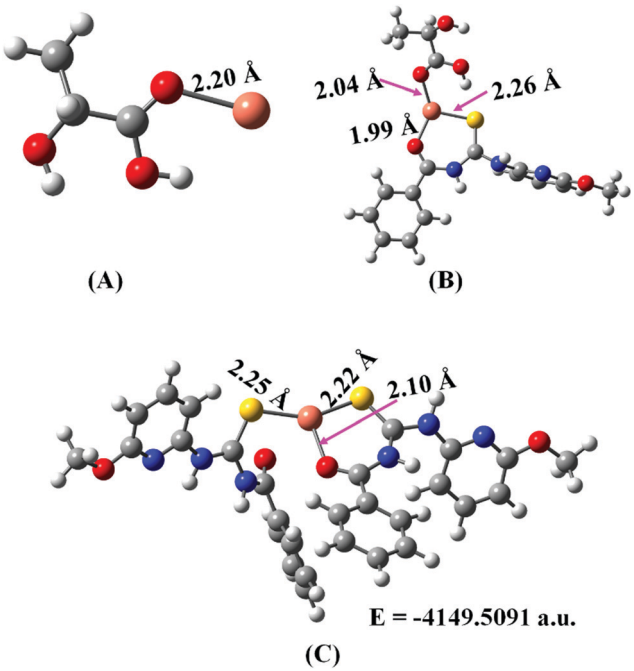

Fig. 9 Optimized structures of (A) lactic acid with Cu^{2+}; (B) Probe **NG1** with Cu^{2+} and lactic acid, and (C) self-associated dimer of **NG1** bonded to single Cu^{2+} ion.

mapped surfaces were generated to elucidate this behavior in terms of charge densities.

Electrostatic potential (ESP) mapped electron density surfaces

The molecular electrostatic potential (MEP) (also called ESP) of a molecular association is correlated with the corresponding partial charges, dipole moment, and chemical reactive sites. The mapping of any molecular system is the way to visualize the relative polarity of the studied molecules. The expression for the ESP at any point r in the space near the molecule is given by

$$V(r) = \sum \frac{z_A}{|R_A - r|} - \int \frac{\rho_{(r')}dr'}{|r' - r|} \quad (2)$$

where Z_A is the charge on the nucleus A studied at R_A and $\rho(r')$ the electron density. For probe **NG1** and complex **NG1** with Cu^{2+} and lactic acid, the electron density iso-surface on which the ESP surfaces were calculated and mapped are shown in (Fig. 10). Recently, ESP mapping has played a remarkable role in the geometrical arrangement, charge density analysis, and polarity of different molecular systems.[48–51] Generally, MESP reflects the relative polarity of the molecule as positive potential indicates the electrophilic sites while adverse potential indicates the nucleophilic attack sites. To visualize the electrophilic and nucleophilic sites in these complexes, the MESP was generated on DFT minimized structures at the B3LYP/6-311++G(d,p) level of theory.

As shown in the top panel of the mapped optimized structure, the potential increases in the colour code. The charge distribution over pristine **NG1** with Cu^{2+} and lactic acid is visualized in the ESP map in Fig. 10. Also, in pristine **NG1**, nitrogen, oxygen, and

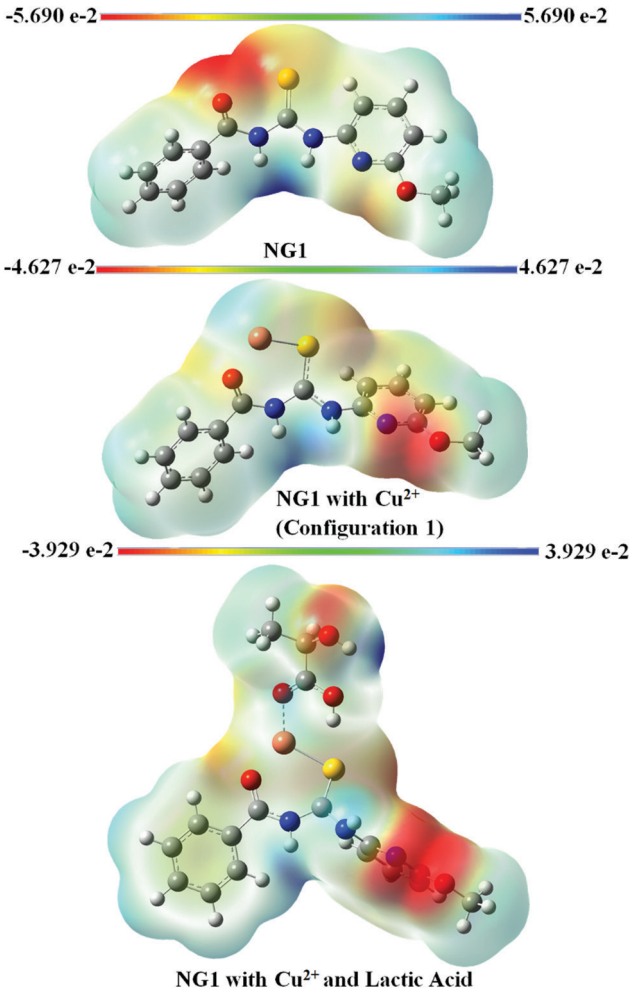

Fig. 10 Electrostatic potential surfaces plotted from the total self-consistent field (SCF) density having iso-value (MO = 0.020000 and density = 0.000400), calculated at the B3LYP level of theory. The red colour indicates the most electronegativity, the blue colour shows the most positive election density and the area of zero potential on the molecular surface is represented by a green colour.

sulphur are the three electronegative atoms, so a negative charge distribution can be noticed over both the oxygen as indicated by the red colour whereas blue colour over the benzene ring and both the nitrogen atoms near sulphur group indicates low electron density (Fig. 10A) as these atoms are less electronegative than oxygen. Shape and charge distribution are found to be considerably different in **NG1** with Cu^{2+} and lactic acid. Positive charge increases (blue colour near the Cu^{2+}) as Cu^{2+} atom attaches with sulphur in comparison with pristine **NG1** and negative charge increases near the oxygen atom which is attached with the $-OCH_3$ group. On going from **NG1**–Cu^{2+} complex to **NG1**–Cu^{2+}-lactic acid, the positive charge increases around the Cu^{2+} as Cu^{2+} binds with the oxygen atom of the carboxylic group of lactic acid. The reason may be due to charge transfer between Cu^{2+} and oxygen atom as it is known that Cu^{2+} forms copper lactate with lactic acid. This result indicates that Cu^{2+} is interacting more with lactic acid than the probe as yellow colour of **NG1**–Cu^{2+} quenches after interacting with lactic acid which is experimentally observed.

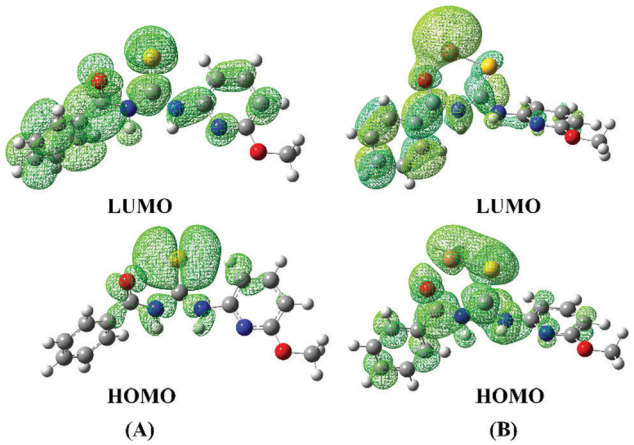

Fig. 11 Molecular orbitals HOMO and LUMO of (A) pristine **NG1** and (B) **NG1** with Cu^{2+}. The orbitals were obtained using an iso-surface value of 0.02 e $Å^{-3}$.

Electronic absorption

Time-dependent density functional theory (TD-DFT) calculated results were used to explain the experimentally measured absorption bands of the complexes **NG1** and **NG1** with Cu^{2+} in the presence of different concentrations of Cu^{2+}. TD-DFT calculations of **NG1** and **NG1** with Cu^{2+} were performed using DFT calculations in the gas-phase. The frontier molecular orbitals of pristine **NG1** and Cu^{2+} are shown in Fig. 11. Quantum chemical calculations show that **NG1** reveals three bands at 427, 325, and 311 nm (experimentally observed at 290 nm in 70% aqueous methanol).

The theoretically calculated absorption at ~325 nm red-shifted when Cu^{2+} was added and absorption appears at ~680 nm, which shows a similar trend as that of experimentally observed absorption bands. Energy bands calculated at ~325 and ~680 nm with oscillator strengths (f) 0.0844 and 0.1445 are due to electronic excitations from HOMO−1 → LUMO and HOMO → LUMO+1 which are attributed to electron transfer from sulphur atom to another part of **NG1** and from sulphur to Cu^{2+} atom, respectively. For both complexes, pristine probe **NG1** and **NG1** with Cu^{2+}-atom, the calculated bands are in good agreement with observed absorption bands and show a similar trend. Overall, a nice correlation is observed between experimental UV-Vis absorption and TD-DFT calculated absorption data.

Experimental

Materials and methods

All the starting materials for **NG1** synthesis were obtained from commercial suppliers and used as received. 2-Amino-6-methoxypyridine and Benzoyl isothiocyanate were purchased from Combi-Blocks, USA. Acetone, THF, and all-metal ions were purchased from Sisco Research Laboratories (SRL), India. $Cu(NO_3)_2{\cdot}2.5H_2O$ and $CuCl_2{\cdot}2H_2O$ were purchased from Sigma. Lactic acid was purchased from Fluka. Moisture sensitive reactions were performed under an atmosphere of nitrogen. All the solvents used for reactions were distilled before use.

All the microscopy and spectroscopy measurements were performed using ultra-pure water obtained from Millipore Direct-Q® 5 UV Water Purification System. R_f was recorded using an Analytical TLC Silica Gel $60F_{254}$ instrument purchased from Merck (Germany). The melting point of **NG1** and its derivatives was recorded using a Visual Melting Range Apparatus (MR-VIS) provided by LABINDIA. ^{1}H NMR (400 MHz) and ^{13}C NMR (100 MHz) spectra were recorded using an Avance III 400 NMR spectrophotometer. Proton chemical shifts were reported in parts per million concerning TMS. HPLC was done using the Waters E2695 instrument. HPLC was performed using ammonium bicarbonate buffer (ABC) with 27 minutes run time and water: ACN as the mobile phase in C-18 Column. LC-MS was obtained using a Waters 2690 LC-MS instrument using ammonium bicarbonate buffer (ABC); 7 minutes run time and water: ACN as the mobile phase in C-18 Column. UV-visible spectra were recorded using a SHIMADZU UV-1900 with a 10 mm quartz cell at 25 °C.

Synthesis of probe NG1

In a three-necked round bottom flask, fitted with a dropping funnel, 50 mL of dry acetone was filled. 5.0 g (27 mM) of 2-amino-6-methoxypyridine was placed followed by the dropwise addition of dry acetone under N2 atmosphere during the constant stirring of the reaction mixture. Next, 7.2 g (44 mM) of benzoyl isothiocyanate was added and the reaction mixture was then allowed to stir for another 2 h at room temperature. The progress of the reaction was monitored through analytical TLC by using ethyl acetate-hexane (3 : 7) as the solvent mixture. After the completion of the reaction, the reaction mixture was poured carefully with stirring into 500 mL cold water and the resulting yellow precipitate of (*N*-((6-methoxypyridin-2-yl)carbamothioyl)benzamide) was separated by suction filtration followed by washing of precipitate with water (3 × 100 mL). The filtrate was further purified by vacuum distillation which yielded the desired product (10.0 g, 34 mmol, and yields 86%) as solid light-yellow material. M.P. 136 °C R_f 0.53, (this material was used in the next step without any further purification). The mass of **NG1** was confirmed using EI-MS. The mass spectrum of **NG1** shows a strong molecular peak at $M^+ + 1 = 287.86$. While the $M^+ + 1$ ion appears for the base peak. Similarly, **NG2** and **NG3** were synthesized using aminopyridine and aniline, respectively, as the substrate {details of **NG2** and **NG3** synthesis are provided in the ESI.† (Scheme S1)}.

Self-assembling properties of NG1

The self-assembling properties of **NG1** were studied using different microscopic techniques at 1 mM concentration in 70% methanol aqueous. The disruption studies were carried out by incubating **NG1** with Cu^{2+} in a 1 : 1 stoichiometric ratio. Similarly, EDTA was added to the complex in a 1 : 1 : 1 stoichiometric ratio (Fig. S20, ESI†).

Field emission-scanning electron microscopy (FE-SEM)

SEM images were taken using a JSM7600F (Jeol) FE-SEM 450 microscope (the accelerating voltage ranging from 1 to 15 kV). SEM samples were prepared on silicon wafers. **NG1** (20 μl of a 1 mM solution) was dispensed and dried at room temperature. The samples were analysed without gold coating under a low vacuum.

Atomic force microscopy (AFM)

Neat and coincubated solutions of **NG1** were imaged using an atomic force microscope. The samples were placed on freshly cleaved muscovite mica surfaces followed by imaging with an AFM (INNOVA, ICON analytical equipment, Bruker, operating under the acoustic AC mode (AAC or tapping mode)), with the aid of a cantilever (NSC 12(c) from MikroMasch, Silicon Nitride Tip) by NanoDrive version 8 software. The force constant was 2.0 N m^{-1}, while the resonant frequency was ~276 kHz. All of the images were taken in the air at rt, with the scan speed of 1.5 lines per s. The data analysis was done using the nanoscope analysis software. The sample-loaded substrates were dried in a dust-free space under a 40 W lamp for 30 min followed by high-vacuum drying and subsequently examined under AFM.

Transmission electron microscopy (TEM)

Transmission electron microscopy (TEM) images were taken using Zeiss Libra 120. 5 μL of **NG1**and **NG1** with Cu^{2+}(1 : 1) solutions at a concentration of 1 mM was dropped on copper grids and dried. Finally, they were stained with uranyl acetate and the excess stain was removed by wiping after 1 minute.

UV visible assay for detection of Cu^{2+}

For colorimetric measurements, stock solutions of 500 ppm **NG1** and 500 ppm $Cu(NO_3)_2{\cdot}2.5\ H_2O$ were prepared. The sensitivity of probe **NG1** for Cu^{2+} and other metal ions was tested by mixing 250 ppm probe **NG1** with 100 ppm metals (100 ppm: Cu^{2+}, Fe^{3+}, Cd^{2+}, Mn^{2+}, Ag^+, Hg^{2+}, Ca^{2+}, Cr^{3+}, K^+, Mg^{2+} and Na^+). The LOD of probe **NG1** was detected by making a complex of 50 ppm : 50 ppm of **NG1** : Cu^{2+}complex. The stoichiometric ratio of the **NG1** : Cu^{2+} complex was determined by adding varying concentrations of Cu^{2+} (0.5–50 ppm) to 50 ppm **NG1**.

Fluorimetric assay for the detection of Cu^{2+} ions and lactic acid

For fluorimetric measurements, 250 ppm of **NG1** stock was added with varying concentrations of Cu^{2+} (0.0001–100 ppm). For lactic acid-mediated quenching, 250 ppm of lactic acid was added to the 250 ppm : 100 ppm **NG1** : Cu^{2+} complex.

UV visible assay for lactate detection

For sensing of lactate ions, a solution of **NG1**–Cu^{2+}complex (50 ppm) was prepared in 70% aqueous methanol. Then solutions of lactic acid were prepared (5000 ppm stock solution) in Milli-Qx water. Then 0 to 500 ppm lactic acid was mixed with of complex solution in a 3 mL vial and the reaction mixtures were incubated for 10 minutes. The UV-Vis spectra of all these solutions were recorded after incubation and those were compared to the spectrum of Cu^{2+}complex of the same concentration but without any lactic acid to ascertain the selectivity.

Computational details

The prediction of certain important molecular properties of the probes **NG1**, **NG2** and **NG3** and their possible complexes with Cu^{2+} and lactic acid are calculated using density functional theory (DFT) calculations. All computational calculations were carried out using the *Gaussian 16* programming package in the present study.[52] *GaussView 6* software was used to generate the input molecular structure and to analyze the output of all calculated results.[53] Geometric optimization calculations were performed in the gas phase using DFT by employing the internally stored 6-311++G(d,p)[54,55] basis sets and the B3LYP hybrid functional method.[56–58] In general, B3LYP is a prominent method and preferable to the HF and MP2 method as it includes Becke's three-parameter exchange with Lee, Yang, and Parr's correlational functional as well as an HF exchange term. DFT calculations using the B3LYP protocol have provided a meaningful and nice correlation with experimental results. In order to analyze the charge transfer from Cu to probe NG1, time-dependent density functional theory (TD-DFT) was also implemented to compute electronic excitation energies and molecular frontier orbitals. Besides, the mapping surfaces for **NG1** with electrostatic potential (ESP) were also shown to better understand the distribution of charges through shape, size and colour code.

Cytotoxic assay

To evaluate the biocompatibility of **NG1**, we performed a standard colorimetric MTT assay. Monkey kidney fibroblast cells were seeded at a density of 5×10^3 cells per well into 96-well plates and maintained in Dulbecco's modified Eagle's medium (DMEM) containing 10% fetal bovine serum (FBS) at 37 °C in a 5% CO_2 incubator. After 24 h, once the cells adhered to a surface, the culture medium was replaced by a fresh culture medium containing varying concentrations of **NG1** compounds and again incubated for 24 hrs at 37 °C in a 5% CO_2 incubator. After incubation, the medium was aspirated and replaced by 100 μL per well of MTT prepared in DMEM medium to a final concentration of 0.5 mg per mL and the plate was incubated furthermore for 4 h at 37 °C in a 5% CO_2 incubator. The formed formazan crystals were solubilized by adding 100 μL of cell culture grade DMSO per well and incubated for 2 h at 37 °C in a 5% CO_2 incubator. The plate was gently shaken, and then the absorbance of purple formazan was recorded at 570 nm using a plate reader.

Cellular sensing of Cu^{2+} ions

Retinal pigmental epithelial cells (RPE1) were seeded at a density of 1.5×10^5 cells per well in Dulbecco's modified Eagle's medium (DMEM) containing 10% fetal bovine serum (FBS) and incubated at 37 °C in a 5% CO_2 incubator for 24 hrs. The medium was replaced with 20 mM HEPES buffer and incubated with **NG1** ± Cu^{2+} ± lactic acid in concentrations of 100 ppm and 250 ppm for 15 min at 37 °C in water. Post incubation, the cells were washed with ice-cold PBS++ to block endocytosis and remove the unbound dye and Cu^{2+} ions. The cells were then fixed using 4% paraformaldehyde for 10 min at room temperature. The fixed coverslips were visualized for dye uptake using Leica SP8 confocal microscope. The cells were excited using 405 nm with a very low laser power (~1% laser power) and the images were acquired using a broad width emission spectrum to capture the maximum of the emitted photons. 50–60 cells were imaged under every condition using the same laser power and imaging conditions.

Data analysis

Image analysis and quantification were performed using Image-J software (nih.gov). 50 cells were randomly selected to perform the quantification. The value of the total fluorescence intensity of each cell was obtained from Image-J. The images were quantified by subtracting the background and measuring the cellular intensities by measuring the areas of the cells and the total cellular intensity. The normalized mean value and standard deviation for each were calculated and plotted in the graph using Prism 7 software and the statistical significance was calculated using a one-way Anova testlusions section.

Conclusions

To conclude, we have reported the self-assembling properties of anacyl thiourea based conjugate **NG1** and its implications as a sensor for the sequential detection of Cu^{2+} and lactic acid. **NG1** self-assembles to fibres which reveal panchromatic emission properties. These fibres get disrupted only by Cu^{2+} ions and their disaggregation led to the formation of yellow colour. The sensitivity and specificity of **NG1** for sensing Cu^{2+} ions are tested using various spectroscopic and biophysical assays. Furthermore, it was found that the sequential addition of lactic acid suppresses the yellow colour formed by the **NG1** + Cu^{2+} complex and its blue fluorescence is also quenched. Since high levels of lactate ions and Cu^{2+} ions are associated with many pathological disorders, the results presented in the manuscript could be of immense importance for the designing of a simple and cost-effective technique for the dual detection of Cu^{2+} and lactate. In addition to the experimental study, DFT calculations were also carried out for assessing the interaction. The comparison of experimental and theoretical results in combination with cell studies ensures a good understanding of the mechanism of the probe along with an immense practical utility for future applications. To the best of our knowledge, this is the first report wherein a probe for the sequential detection of copper and lactate has been designed and the effect of aggregation properties of the sensor has been studied to decipher its photophysical characteristics.

Author contributions

The manuscript was written by the contribution of all authors. NG proposed the application of probe and coordinated the overall project including drafting of the manuscript and its correspondence. VK synthesized the probes **NG1**, **NG2** and

NG3. VK, BK and CK did UV. Fluorescence and self-assembly studies were carried out by the BK and VK jointly. DKS and DKP performed DFT calculations, structural part was discussed by DKP and electronic properties of all the probes and their complexes were explained by DKS. SK and DB devised cell culture experiments. SK performed the cellular uptake and quantification of dye uptake in cells. All the authors discussed the results and contributed to manuscript drafting.

Funding source

The work was supported by the DST SERB extramural research fund (Project No. EMR/2016/003186) received by Dr Nidhi Gour and DST-SERB Ramanujan Fellowship to Dhiraj Bhatia. DKS acknowledges financial support from the SERB-DST ECR project ''ECR/2016/001289''.

Conflicts of interest

There is no conflict of interest to declare.

Acknowledgements

NG thanks Indrashil University and Institute of Advanced research Gandhinagar for the infrastructure support. NG, VK, and CKP greatly acknowledge support from DST and SERB research grant (EMR/2016/003186) for funding and fellowships. BK thanks Indrashil university for funding and infrastructure support. DKP is grateful to DST, India for providing financial support under the INSPIRE Fellowship No. IF170625. DS thanks GSBTM for the fellowship. DB thanks Central Imaging Facility, (CIF) at IITGN for confocal microscopy, XRD and the initial seed funding from IITGN to DB. Mr. Ashadul Haque (IITGn) is thanked for helping in XRD analysis. Ramesh Singh Chilwal and Dr K. B. Joshi (Sagar University) are thanked for their help in AFM imaging. NG also gratefully acknowledges Prof Ehud Gazit (Tel Aviv University, Israel) and his PhD student DorZaguri for useful discussion and experimental support.

Notes and references

1 Y. Jiao, J.-F. Xu, Z. Wang and X. Zhang, *ACS Appl. Mater. Interfaces*, 2017, **9**, 22635–22640.
2 N. S. Sariciftci, L. Smilowitz, A. J. Heeger and F. Wudl, *Science*, 1992, **258**, 1474–1476.
3 E. Wang, J. W. Lam, R. Hu, C. Zhang, Y. S. Zhao and B. Z. Tang, *J. Mater. Chem. C*, 2014, **2**, 1801–1807.
4 N. Lu, X. Gao, M. Pan, B. Zhao and J. Deng, *Macromolecules*, 2020, **53**, 8041–8049.
5 B. Zhang, H. Wu, Z. Wang, A. Qin and B. Z. Tang, *J. Mater. Chem. C*, 2020, **8**, 4754–4762.
6 Y. Hong, J. W. Lam and B. Z. Tang, *Chem. Soc. Rev.*, 2011, **40**, 5361–5388.
7 L. Xu, Z. Wang, R. Wang, L. Wang, X. He, H. Jiang, H. Tang, D. Cao and B. Z. Tang, *Angew. Chem., Int. Ed.*, 2020, **59**, 9908–9913.
8 Y. Hong, S. Chen, C. W. T. Leung, J. W. Y. Lam, J. Liu, N.-W. Tseng, R. T. K. Kwok, Y. Yu, Z. Wang and B. Z. Tang, *ACS Appl. Mater. Interfaces*, 2011, **3**, 3411–3418.
9 T. J. Meyer, *Pure Appl. Chem.*, 1986, **58**, 1193–1206.
10 G. Zhang, G. Kim and W. Choi, *Energy Environ. Sci.*, 2014, **7**, 954–966.
11 X. Y. Shen, Y. J. Wang, E. Zhao, W. Z. Yuan, Y. Liu, P. Lu, A. Qin, Y. Ma, J. Z. Sun and B. Z. Tang, *J. Phys. Chem. C*, 2013, **117**, 7334–7347.
12 H. Sunahara, Y. Urano, H. Kojima and T. Nagano, *J. Am. Chem. Soc.*, 2007, **129**, 5597–5604.
13 X. Cao, Y. Li, Y. Yu, S. Fu, A. Gao and X. Chang, *Nanoscale*, 2019, **11**, 10911–10920.
14 X. Cao, Y. Li, Q. Han, A. Gao, B. Wang, X. Chang and J.-T. Hou, *J. Mater. Chem. C*, 2020, **8**, 4058–4064.
15 D. Zhai, W. Xu, L. Zhang and Y.-T. Chang, *Chem. Soc. Rev.*, 2014, **43**, 2402–2411.
16 M. Deiana, K. Chand, J. Jamroskovic, I. Obi, E. Chorell and N. Sabouri, *Angew. Chem., Int. Ed.*, 2020, **132**, 906–912.
17 J. Yang, C.-C. Dong, X.-L. Chen, X. Sun, J.-Y. Wei, J.-F. Xiang, J. L. Sessler and H.-Y. Gong, *J. Am. Chem. Soc.*, 2019, **141**, 4597–4612.
18 D. Su, C. L. Teoh, L. Wang, X. Liu and Y.-T. Chang, *Chem. Soc. Rev.*, 2017, **46**, 4833–4844.
19 X. Li, H. Jiang, Z. Luo, Y.-T. Chang and L. Zhang, *Chem. Commun.*, 2016, **52**, 9086–9088.
20 L. K. Kumawat, A. A. Abogunrin, M. Kickham, J. Pardeshi, O. Fenelon, M. Schroeder and R. B. Elmes, *Front. Chem.*, 2019, **7**, 354.
21 X. Cao, Y. Li, A. Gao, Y. Yu, Q. Zhou, X. Chang and X. Hei, *J. Mater. Chem. C*, 2019, **7**, 10589–10597.
22 X. Cao, N. Zhao, A. Gao, Q. Ding, Y. Li and X. Chang, *Langmuir*, 2018, **34**, 7404–7415.
23 M. Reches and E. Gazit, *Science*, 2003, **300**, 625–627.
24 E. Gazit, *Prion*, 2007, **1**, 32–35.
25 R. Scherzer-Attali, R. Pellarin, M. Convertino, A. Frydman-Marom, N. Egoz-Matia, S. Peled, M. Levy-Sakin, D. E. Shalev, A. Caflisch and E. Gazit, *PLoS One*, 2010, **5**, e11101.
26 A. Paul, B.-D. Zhang, S. Mohapatra, G. Li, Y.-M. Li, E. Gazit and D. Segal, *Front. Mol. Biosci.*, 2019, **6**, 16.
27 W. Zhang, T. Wang, Z. Pei, D. S. Miller, X. Wu, M. L. Block, B. Wilson, W. Zhang, Y. Zhou and J.-S. Hong, *FASEB J.*, 2005, **19**, 533–542.
28 Y. Chang, J. Fu, K. Yao, B. Li, K. Xu and X. Pang, *Dyes Pigm.*, 2019, **161**, 331–340.
29 K. Aou, S. Kang and S. L. Hsu, *Macromolecules*, 2005, **38**, 7730–7735.
30 A. Saeed, R. Qamar, T. A. Fattah, U. Flörke and M. F. Erben, *Res. Chem. Intermed.*, 2017, **43**, 3053–3093.
31 G. Singh and S. Rani, *Eur. J. Inorg. Chem.*, 2016, 3000–3011.
32 S. Suganya and S. Velmathi, *Sens. Actuators, B*, 2015, **221**, 1104–1113.

33 W. M. Khairul, M. F. A. Hasan, A. I. Daud, H. M. Zuki and M. A. Kadir, *Malaysian Journal of Analytical Sciences*, 2015, **20**(1), 73–84.
34 Y. R. Sadaphal and S. S. Gholap, *Sens. Actuators, B*, 2017, **253**, 173–179.
35 S. Liu, J. Kang, X. Cao and X. Yue, *Spectrochim. Acta, Part A*, 2016, **153**, 471–477.
36 N. Gour, C. Kanth P, B. Koshti, V. Kshtriya, D. Shah, S. Patel, R. Agrawal-Rajput and M. K. Pandey, *ACS Chem. Neurosci.*, 2018, **10**, 1230–1239.
37 N. Gour and S. Verma, *Soft Matter*, 2009, **5**, 1789–1791.
38 N. Gour, D. Kedracki, I. Safir, K. X. Ngo and C. Vebert-Nardin, *Chem. Commun.*, 2012, **48**, 5440–5442.
39 N. Gour, J. N. Abraham, M. Chami, A. Castillo, S. Verma and C. Vebert-Nardin, *Chem. Commun.*, 2014, **50**, 6863–6865.
40 J. N. Abraham, N. Gour, S. Bolisetty, R. Mezzenga and C. Nardin, *Eur. Polym. J.*, 2015, **65**, 268–275.
41 N. Gour, S. Mondal and S. Verma, *J. Pept. Sci.*, 2011, **17**, 148–153.
42 N. Gour, V. Kshtriya, S. Gupta, B. Koshti, R. Singh, D. Patel and K. B. Joshi, *ACS Appl. Bio. Mater.*, 2019, **2**, 4442–4455.
43 E. Gazit, *FASEB J.*, 2002, **16**, 77–83.
44 J. M. Aguirre, A. Gutiérrez and O. Giraldo, *J. Braz. Chem. Soc.*, 2011, **22**, 546–551.
45 P. Singh, S. K. Brar, M. Bajaj, N. Narang, V. S. Mithu, O. P. Katare, N. Wangoo and R. K. Sharma, *Mater. Sci. Eng., C*, 2017, **72**, 590–600.
46 D. Bhatia, S. Surana, S. Chakraborty, S. P. Koushika and Y. Krishnan, *Nat. Commun.*, 2011, **2**, 1–8.
47 D. Bhatia, S. Mehtab, R. Krishnan, S. S. Indi, A. Basu and Y. Krishnan, *Angew. Chem., Int. Ed.*, 2009, **48**, 4134–4137.
48 A. Bharti, P. Bharati, R. Dulare, M. Bharty, D. K. Singh and N. Singh, *Polyhedron*, 2013, **65**, 170–180.
49 D. Majumdar, S. Dey, D. Das, D. K. Singh, S. Das, K. Bankura and D. Mishra, *J. Mol. Struct.*, 2019, **1185**, 112–120.
50 P. Sanchora, D. K. Pandey, D. Rana, A. Materny and D. K. Singh, *J. Phys. Chem. A*, 2019, **123**, 4948–4963.
51 D. K. Pandey, H. L. Kagdada, A. Materny and D. K. Singh, *J. Mol. Liq.*, 2021, **322**, 114538.
52 M. J. Frisch, G. W. Trucks, H. B. Schlegel, G. E. Scuseria, M. A. Robb, J. R. Cheeseman, G. Scalmani, V. Barone, G. A. Petersson, H. Nakatsuji, X. Li, M. Caricato, A. V. Marenich, J. Bloino, B. G. Janesko, R. Gomperts, B. Mennucci, H. P. Hratchian, J. V. Ortiz, A. F. Izmaylov, J. L. Sonnenberg, D. Williams-Young, F. Ding, F. Lipparini, F. Egidi, J. Goings, B. Peng, A. Petrone, T. Henderson, D. Ranasinghe, V. G. Zakrzewski, J. Gao, N. Rega, G. Zheng, W. Liang, M. Hada, M. Ehara, K. Toyota, R. Fukuda, J. Hasegawa, M. Ishida, T. Nakajima, Y. Honda, O. Kitao, H. Nakai, T. Vreven, K. Throssell, J. A. Montgomery Jr., J. E. Peralta, F. Ogliaro, M. J. Bearpark, J. J. Heyd, E. N. Brothers, K. N. Kudin, V. N. Staroverov, T. A. Keith, R. Kobayashi, J. Normand, K. Raghavachari, A. P. Rendell, J. C. Burant, S. S. Iyengar, J. Tomasi, M. Cossi, J. M. Millam, M. Klene, C. Adamo, R. Cammi, J. W. Ochterski, R. L. Martin, K. Morokuma, O. Farkas, J. B. Foresman and D. J. Fox, 2016.
53 T. Keith and J. M. Millam, *GaussView*, Semichem Inc., Shawnee Mission, KS, 2016.
54 M. A. McAllister, *THEOCHEM*, 1998, **427**, 39–53.
55 D. K. Singh, S. Cha, D. Nam, H. Cheong, S. W. Joo and D. Kim, *ChemPhysChem*, 2016, **17**, 3040–3046.
56 A. D. Becke, *Phys. Rev. A: At., Mol., Opt. Phys.*, 1988, **38**, 3098.
57 A. D. Becke, *J. Chem. Phys.*, 1992, **96**, 2155–2160.
58 D. K. Pandey, H. L. Kagdada, A. Materny and D. K. Singh, *J. Phys. Chem. A*, 2021, DOI: 10.1021/acs.jpca.0c10912.
59 A. Ala, A. P. Walker, K. Ashkan, J. S. Dooley, and M. L. Schilsky, Wilson's disease, *The Lancet*, 2007, **369**(9559), 397–408, DOI: 10.1016/S0140-6736(07)60196-2.

